JOURNAL OF GEOPHYSICAL RESEARCH, VOL. 96, NO. E4, PAGES 20,933–20,946, NOVEMBER 25, 1991

Corona Structures on Venus: Models of Origin

ELLEN R. STOFAN,[1] DUANE L. BINDSCHADLER,[2] JAMES W. HEAD, AND E. MARC PARMENTIER

Department of Geological Sciences, Brown University, Providence, Rhode Island

Coronae on Venus are circular to elongate structures with maximum widths of 150-1000 km characterized by annuli of concentric ridges surrounding complex interiors. The features have raised topography relative to the surroundings, they are associated with volcanic activity, and most are partially surrounded by a peripheral trough. Variations in morphology between individual coronae are due to differences in their stage of evolution and/or differences in the relative significance of the geologic processes that occur in each stage. We examine models for three processes that may be involved in corona origin and evolution: (1) a hotspot or rising mantle diapir model, (2) a sinking mantle diapir model, and (3) gravitational relaxation of topography. Rising mantle diapirs are caused by heating at depth (e.g., hotspot), while sinking mantle diapirs may result from cooling or a phase change causing increased density and negative buoyancy at the base of the lithosphere. The hotspot model is most consistent with the major characteristics of coronae, with gravitational relaxation occurring as a modificational process. The sinking mantle diapir would produce dominant central compression that has not been observed at coronae; however, higher-resolution image and altimetry data from Magellan can be used to distinguish more fully between the two models. Coronae in various states of formation and degradation can be identified in the Venera 15/16 data, suggesting that the process may be continuing today.

INTRODUCTION

The Venera 15/16 mission to Venus revealed a number of terrain types and classes of features of unknown origin. Among these, coronae are closed or partly closed circular to elongate structures surrounded by an annulus of concentric ridges [*Pronin and Stofan*, 1990] (Figure 1). The features, first described by *Barsukov et al.* [1986], have maximum widths of 150-1000 km and interiors that are geologically complex. Tectonic features characteristic of the interior of coronae include ridges and grooves in radial, concentric, oblique, and/or chaotic patterns. Volcanic features such as domes, central edifices, and flowlike features are also common in the interior of coronae. The annuli of ridges surrounding the structures are discontinuous and vary in width, generally composing 15-60% of the maximum radius of a corona. The general morphology, evidence of imbrication within the annuli, and similarities to features of compressional origin indicate that the majority of annuli ridges are compressional in origin [*Stofan and Head*, 1990; *Pronin and Stofan*, 1990]. Volcanic flowlike features frequently overlap and/or surround the rim, which is also frequently cut by regional tectonic lineaments [*Stofan and Head*, 1990]. Coronae are generally characterized by relatively raised topography (<1.5 km above the surrounding region), and are sometimes surrounded by an exterior moat [*Basilevsky et al.*, 1986; *Stofan and Head*, 1986, 1990]. Several modes of origin for coronae have been suggested including hotspots [*Basilevsky et al.*, 1986], ring dikes [*Masursky*, 1987] and rising and sinking diapirism [*Stofan et al.*, 1987]. All models of origin must account for the raised topography of coronae, which may have undergone modification through processes such as gravitational relaxation [*Stofan et al.*, 1988].

We assess the mantle diapir models of corona origin using the basic characteristics of coronae: relatively raised topography, annuli of compressional ridges, volcanism, and peripheral trough. Both rising and sinking diapirs are modeled quantitatively. Thermal instabilities in the mantle (hotspots or rising diapirs) may form resulting in uplift and volcanism at the surface. Sinking diapirs may result from cooling or a phase change causing increased density and delamination at the base of the lithosphere. The effects of gravitational relaxation on the raised topography produced by these models are also assessed. Predictions of the topography and resulting stresses produced by these models are then compared to observed coronae characteristics.

BACKGROUND

The morphology, topography, and general characteristics of coronae provide important information on their origin and evolution. Twenty-one coronae that fit the definition given above have been described by *Pronin and Stofan* [1990], while a group of coronae in the Mnemosyne Regio region were characterized by *Stofan and Head* [1990]. Three classes of coronae have been identified: symmetrical, asymmetrical, and subdued [*Pronin and Stofan*, 1990]. Symmetrical coronae are characterized by circular to oval form, with the annulus surrounding at least 75% of the structure. Asymmetrical coronae are similar in interior morphology to the symmetrical class but are

[1]Now at Jet Propulsion Laboratory, Pasadena, California.
[2]Now at Department of Earth and Space Sciences, University of California, Los Angeles.

Paper number 91JE02218.
0148-0227/91/91JE-02218$05.00

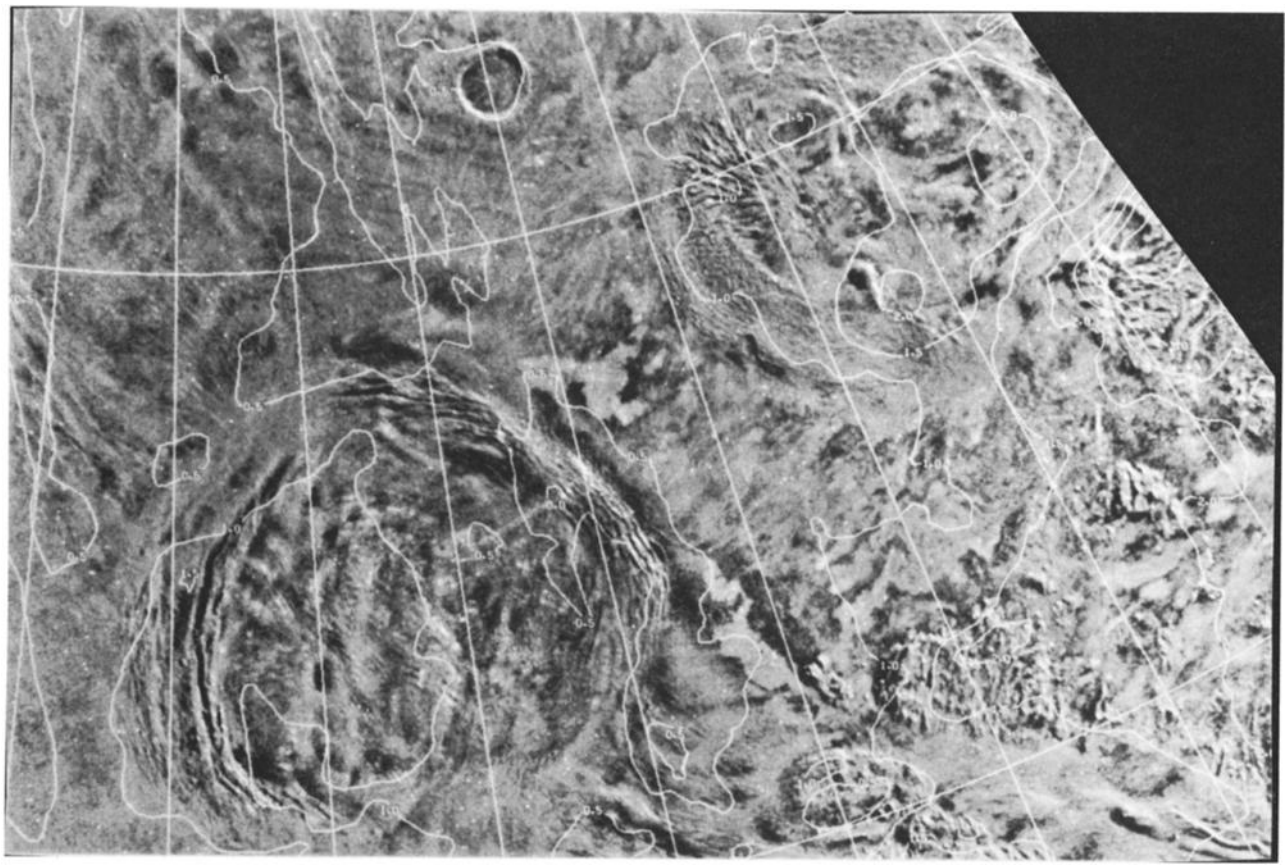

Fig. 1. Venera 15/16 radar image of Anahit Corona, centered at 63°N, 264°. The corona, approximately 350 km across, has an interior characterized by smooth plains, domes, and a volcanic edifice. The corona Pomona is seen to the northeast.

asymmetrical about a central axis or have an annulus on only one side of the structure. Subdued coronae are also similar in general morphology to the symmetrical class, but their interiors are dominated by smooth plains, and the annuli have a flooded and embayed appearance.

Corona Annulus

The symmetrical, asymmetrical, and subdued coronae are all characterized by annuli of concentric ridges that compose 15-60% of the maximum width of the structure (Figure 2). Ridges within the annulus are spaced 5-15 km apart [*Stofan and Head*, 1986; Kryuchkov, 1988*a*], similar to ridge spacing in the banded terrain surrounding Lakshmi Planum [*Solomon and Head*, 1984] which is thought to be controlled by the thickness of a surface elastic layer in the crust. Some evidence of imbrication can be seen within the annuli, and the annuli are similar in general morphology to features of compressional origin found in Akna and Freyja Montes [*Campbell et al.*, 1983; *Crumpler et al.*, 1986] and some ridge belts [*Kryuchkov*, 1988*b*; *Frank and Head*, 1988]. The general morphology and topography of the majority of ridges within the annulus strongly suggest that they are compressional in origin [*Stofan and Head*, 1990; *Pronin and Stofan*, 1990].

Associated Tectonic Features

The interiors of coronae are also characterized by tectonic features, some of regional origin and some associated directly with corona formation and evolution (Figure 2). Both extensional grooves and compressional tectonic ridges can be identified in the interior of coronae, along with some tectonic lineaments of unknown origin. Some extensional features, such as a group of lineaments in Bachue Corona, lie along the highest topography within the corona and appear to be associated with uplift of topography. Many coronae (e.g., Rananeida, Feronia) are characterized by throughgoing compressional ridges that appear to be related to regional tectonic activity rather than coronae formation and/or evolution [*Stofan and Head*, 1990]. Other lineaments within coronae appear to be related to small volcanic edifices (< 50 km in diameter), such as at Otau and Pomona coronae. These lineaments surrounding the volcanic edifices may be tectonic in origin or may be volcanic features. Nightingale and Fakahotu coronae are also characterized by chaotic terrain, consisting of orthogonal to obliquely intersecting ridges. Chaotic terrain occurs in the inner annulus and may result from later modification (i.e., gravity sliding) within the annulus [*Pronin and Stofan*, 1990]. In general, unless tectonic lineaments are associated with regional

IDEALIZED CORONA SKETCHMAP

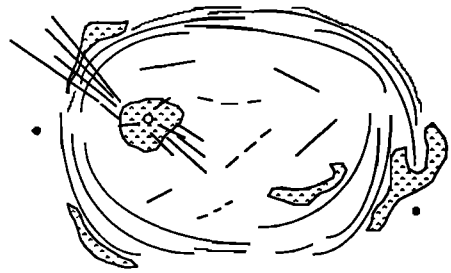

FEATURE	CHARACTERISTICS
ANNULUS	Compose 15-60% of the maximum radius of a corona. Discontinuous, varies in width, often asymmetrical. Ridges spaced 5-15 km apart, imbrication seen. Interpreted as compressional in origin.
INTERIOR RIDGES	Less than 100 km long, radar-bright and dark. Of compressional, extensional and unknown origin. In radial, concentric and oblique orientations.
INTERIOR GROOVES	Randomly oriented, less than 100 km long. Graben 5-20 km wide. Interpreted as extensional in origin.
CHAOTIC TERRAIN	Ridges and grooves intersecting in orthogonal to oblique orientations. Occur in 2 coronae, interpreted as complex deformation of annulus.
DOME	5-15 km diameter, some with summit pits. Located in annulus, interior and exterior. Interpreted as volcanic in origin.
FLOW	Up to 100's of kms long, radar-bright and dark. Few sources identified, interpreted as volcanic in origin.
EDIFICE	30-50 km in diameter, summit pits or calderas. Flows and radial ridges surround the edifices, which generally lie along tectonic trends. Interpreted as volcanic in origin.

Fig. 2. Idealized sketch map of a corona showing possible associated tectonic and volcanic features.

tectonic activity or local volcanic activity within a corona, the lineaments do not cut the annulus and appear to be produced by extensional and/or compressional forces related to corona evolution.

Associated Volcanism

All coronae are associated with volcanic activity, occurring at various times throughout their evolution. Small domes (10-15 km in diameter) are found in the interior, in the annulus, and in the region surrounding coronae (Figure 2). *Barsukov et al.* [1986], noting the presence of summit craters on many of the small domes in the Venusian plains, interpreted the domes to be volcanic in origin, possibly produced by strombolian-type eruptions [*Head and Wilson,* 1986]. Analysis of the dome population for the seven coronae in the Mnemosyne Regio area shows that the population of domes inside the coronae is higher than in the surrounding region, indicating that formation of the domes is related to coronae origin and evolution, as well as regional volcanic activity. Coronae are also characterized by volcanic flows, found in the interior and overlapping and surrounding the rim (Figure 2). Flows frequently pond in the peripheral trough and inside the coronae in topographic lows bordering the annulus. Aside from some small volcanic edifices, no clear sources for the flows can be identified. Some coronae, such as Otau, Pomona, and Feronia, are also associated with small volcanic edifices, 20-50 km in diameter (Figure 2). The edifices always lie along lineament trends that cut the annulus and appear to be related to regional tectonic activity. The volcanic edifices are surrounded by flows and apparent tectonic ridges or dikes. Coronae differ significantly from most volcanic complexes in that they are not characterized by a dominant central edifice, indicating that coronae have had a more complex volcanic evolution.

Topography

Both Pioneer Venus and Venera 15/16 topographic data indicate that coronae are generally raised <1.5 km

PIONEER VENUS TOPOGRAPHIC PROFILES

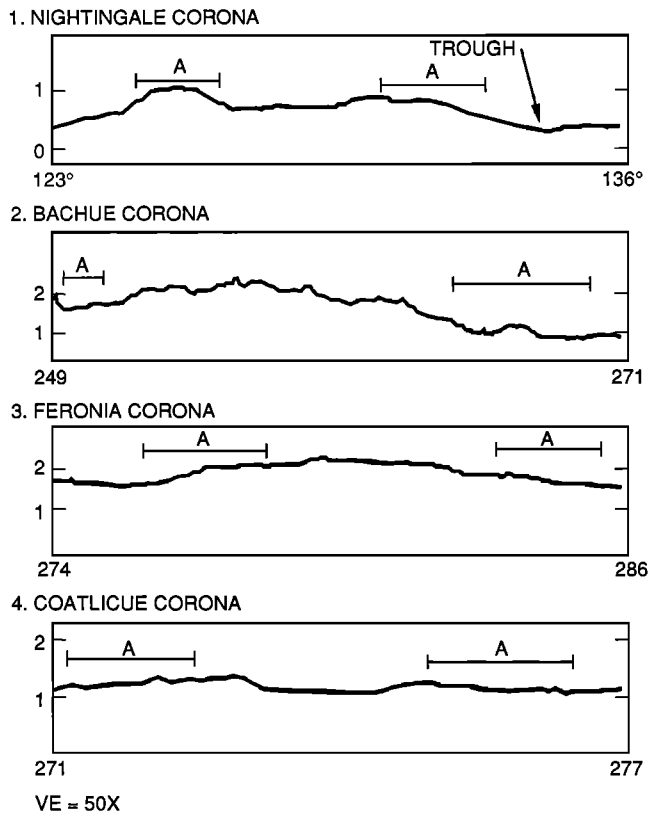

Fig. 3. Topographic profiles across several coronae based on Pioneer Venus altimetry measurements. Profile 1, Nightingale Corona; profile 2, Bachue Corona; profile 3, Feronia Corona; profile 4, Coatlicue Corona. The profiles were created with the 1985 NSSDC Pioneer Venus data set (footprint size in the region is approximately 100 x 100 km, vertical accuracy about 200 m [*Pettengill et al.*, 1980]). The profiles show that some coronae are characterized by relatively domelike topography, while others are characterized by a central topographic low. Approximately half of coronae mapped in the northern hemisphere are at least partially surrounded by a peripheral trough.

above the surrounding region. Profiles across several coronae are seen in Figure 3. The central region of many coronae is at a lower elevation than the annulus (profiles 1, 4, Figure 3). The annulus corresponds to raised or sloping topography, with ridges within the annulus generally paralleling topographic trends. Over half of coronae are also characterized by a peripheral trough (Figure 4), approximately 500 m deep and 50-75 km wide in the case of the Mnemosyne coronae group. The trough generally lies outside the annulus.

Evolutionary Sequence

Stofan and Head [1990] examined the morphology of seven coronae in the Mnemosyne Regio area and derived a general evolutionary sequence for these features (Figure 4). Comparisons to the morphology of a large number of coronae [*Pronin and Stofan,* 1990] provide further support for this sequence. Regional tectonic and volcanic activity were generally found to precede corona formation. The initial stage of corona formation (1, Figure 4) involves uplift of the surface, volcanic activity, and construction.

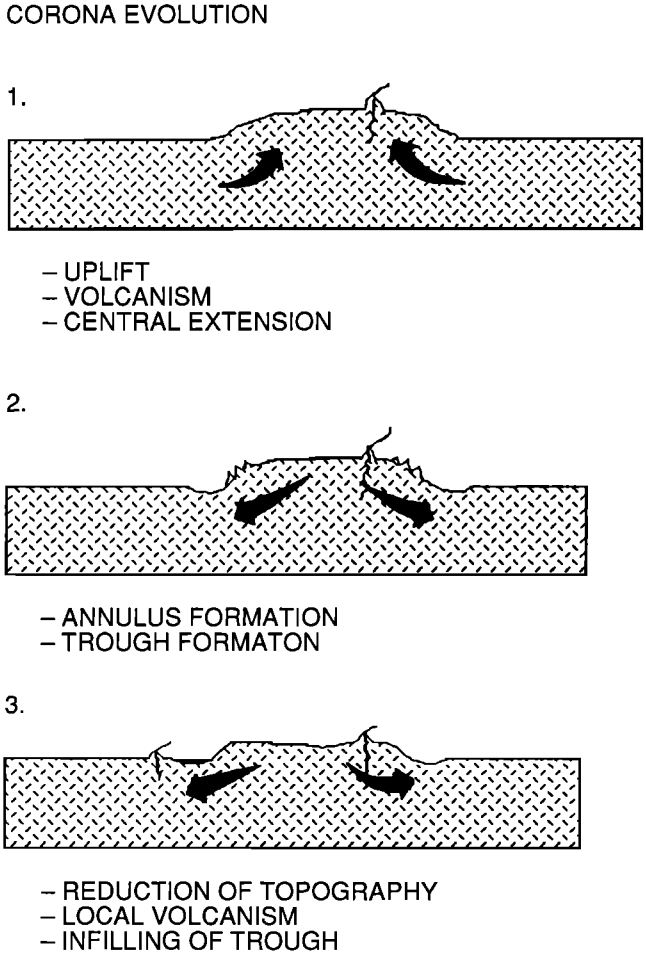

Fig. 4. Generalized sequence of events of corona evolution. In the first stage, coronae are characterized by uplift, volcanism, and central extension. Annulus and trough formation occur in the second stage, with reduction of topography, local volcanism, and infilling of the trough occurring in the third stage.

Corona such as Bachue exhibit high topography and central extension that are consistent with domal uplift. Coronalike volcanic structures such as Sekmet Mons and 58°N, 255° provide evidence that uplift and volcanic construction precede annulus and trough formation. These volcanic structures have been interpreted as protocoronae [*Stofan and Head,* 1990]. In the second stage (2, Figure 4), volcanism continues combined with formation of the annulus and peripheral trough. Last (3, Figure 4), topographic degradation and volcanism are the dominant processes, with covering of the annulus and infilling of the trough by local volcanic activity. Late stage regional tectonic activity postdates corona formation, with bands of lineaments frequently cutting coronae annuli. Volcanism, in the form of small volcanic edifices discussed above, tends to concentrate along these lineament bands. Despite the general similarities between coronae that allow them to be classified as a group, significant differences in morphology exist between individual coronae. We interpret these differences to reflect the differing amounts and significance of the processes discussed above in the formation of each corona. For example, some coronae have been significantly overprinted by regional tectonic activity (e.g., Rananeida), while others postdate much of the regional deformation (e.g., Otau). All coronae appear to follow the evolutionary sequence described above, but the stage that different coronae are at may vary as well as the relative significance of the processes that occur in each stage.

Summary

Coronae appear to form by uplift and volcanic construction, followed by formation of the annulus and peripheral trough. Both extensional and compressional features can be found in the interior of the structures, with volcanism occurring throughout their evolution. The interior of some coronae are also topographically lower than the annulus, which does not always completely surround the corona. The basic characteristics of coronae that must be accounted for in any model of origin include relatively raised topography, annuli of compressional ridges, interior volcanic and tectonic activity, presence of a peripheral trough, and the evolutionary sequence described above. These general characteristics suggest some basic processes related to thermal perturbations, diapirism, and gravitational relaxation. We have pursued models of these processes in order to test whether they produce surface features and sequences similar to that observed for coronae. In this paper, we discuss three analytical models that may be significant in corona origin and evolution: mantle diapir models (both rising and sinking anomalies) and gravitational relaxation of a plateau and dome.

Mantle Diapir Models

Diapirism involves the rising or sinking of material. Density contrasts may result from heating and partial melting, causing upward movement of

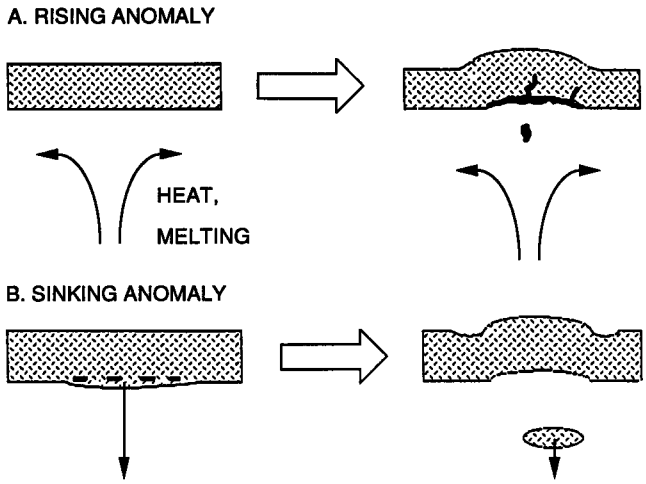

Fig. 5. (*a*) Idealized rising anomaly model of corona origin. A thermal anomaly or hotspot results in partial melting, with lighter buoyant material rising causing uplift and volcanism at the surface. (*b*) Idealized sinking anomaly model of corona origin. A sinking diapir may form due to a phase change produced by thickening of the lithosphere below a critical depth or cooling instabilities at the base of the lithosphere

material (Figure 5*a*). Conversely, cooling or a phase change may cause the density of material to increase, resulting in downward motion (Figure 5*b*). We have formulated a model to study the effects on the surface of both upward and downward motion from the interior of a planet.

Hotspot or Rising Mantle Diapir Model

First, we examine the topography and deformation that are predicted to result from the upward movement of a diapiric body in the Venus mantle. The crust and mantle are treated as a linear viscous half-space that is layered in both density and viscosity, following the approach of *Bindschadler and Parmentier* [1990] (Figure 6). In all models, we assume a 10% density contrast between the crust and mantle, and a crustal density of 3000 km/m^3. Effective linear viscosities for individual layers are obtained from flow laws for diabase [*Shelton and Tullis,* 1981], representing crustal rocks, and olivine [*Goetze,* 1978], representing mantle rocks. Temperatures are assumed to follow an error function distribution with depth, appropriate for a thermal boundary layer. Near the surface, such a distribution is approximately linear but at depth approaches an asymptotic value appropriate to a convective system (1500 K). Flow is driven by an axisymmetric density anomaly within the halfspace, representing the rising diapiric body. We take the rising body to have a stress magnitude of about 30 MPa (the stress necessary to support 1 km of topography). A number of shapes were examined for the shape of the diapiric body, including spherical, multilayered shapes. Results were found to be insensitive to choice of diapir shape, and a Gaussian function was used in the results described below, largely for computational convenience.

In this multiple-layered linear model, solutions to the equations of flow are fully determined by boundary conditions on the half-space and matching conditions between individual layers. Velocities are required to vanish at great depths ($z \rightarrow \infty$), while at the surface shear stresses vanish and vertical normal stresses are those due to topography. Horizontal and vertical components of velocity and shear and vertical normal stresses are required to be continuous across viscosity interfaces within the halfspace, except at the crust-mantle boundary and at the location of the density anomaly. Here, vertical normal stresses are discontinuous by amounts dependent upon the deflection of the crust-mantle boundary and the magnitude of the density anomaly, respectively. In practice, the density anomaly representing the rising diapir is deconvolved into individual harmonics using two-dimensional fast Fourier transforms (FFT's). Boundary and matching conditions form a set of linear equations for each harmonic which is solved using matrix inversion methods and whose solution yields constants of the equations of flow. We describe results of the various models in terms of surface topography and style of deformation. Deformation is examined by calculating principal stresses at the surface at different times during the rise of the diapiric body. Stresses are calculated directly from the equations of flow. Following Anderson's theory [1951], fault types are determined by the orientations of greatest and least compressive stresses.

Strictly speaking, the above model only allows us to consider the effects of a steady (fixed in space) source of mantle flow. In order to consider dynamic effects, continuous movement of the diapir is simulated by placing the diapir at a depth d for a time interval Δt that is short compared to the characteristic response time of the crust [*Bindschadler and Parmentier,* 1990] and calculating accumulated topography at the surface

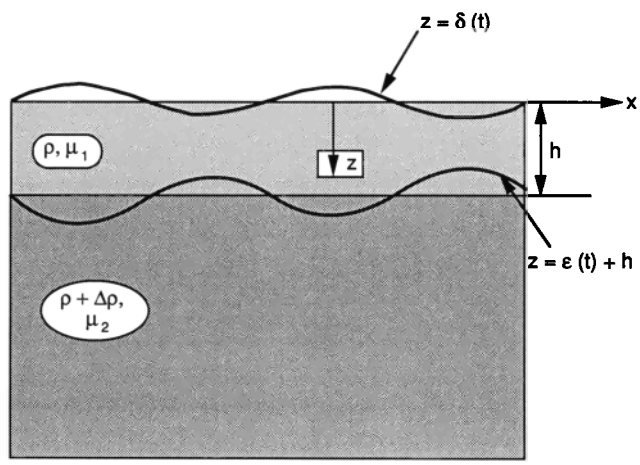

Fig. 6. Schematic of the model used for the rising and sinking diapir models and the gravitational relaxation model, [after *Bindschadler*, 1990]. In the simplified case shown, the half-space is stratified in both density and viscosity, with topography at the surface and at $z = h$ (h = upper layer thickness) represented by harmonic functions ($d(x, t) = F(t)$ cos kx, $e(x,t) = G(t)$ cos kx, where k is the wavenumber and F and G are time-dependent amplitudes of the topography at the surface (F) and along the interface (G)). The case described in the text utilized multiple layers with viscosities varying according to flow laws for diabase and olivine.

and the crust-mantle boundary. The diapir is then moved a distance $\Delta z = w\,\Delta t$, where w is determined from Stoke's law and the resulting Δz is much less than the crustal thickness. At each new location of the diapir, additional topography is added to that which has already accumulated. Results were tested for convergence by halving the time interval and comparing topography and surface stresses and were found to be identical within 1%.

In this model, the response of the surface to a rising diapiric body is most strongly affected by the strength (viscosity) structure of the crust and uppermost mantle, or the rheological lithosphere. The strength of these layers is most strongly affected by the crustal thickness and thermal gradient and, to some extent, is also a function of the characteristic value of deviatoric stress used to obtain linear viscosities from flow laws [*Grimm and Solomon,* 1988]. We have examined model results for crustal thickness values of 10 and 30 km; surface thermal gradients of 10, 20, and 30 K km^{-1}; and characteristic stress values of 10 and 25 MPa. These values represent likely limits on the model. In all of these runs, the diapir was placed initially at a depth of 300 km and was allowed to rise to a depth of approximately 100 km. Calculations were halted at that point because of the likelihood that the interaction between the diapir and the overlying lithosphere would result in significant flattening of the diapir and subsequent alteration of the flow field.

The nominal case of the model was run with a 10-km-thick crust, a 20 K km^{-1} surface thermal gradient, and a characteristic stress value of 10 MPa (Figure 7). The rising mantle diapir or hotspot results in uplift of the surface, with the magnitude of the uplift increasing and the width decreasing as the diapir approaches the surface (Figure 7*a*). An increase in the thermal gradient results in decreasing topographic uplift due to weakening of the lithosphere permitting crustal thinning to begin before the diapir reaches near-surface levels. An increase in the crustal thickness similarly reduces the amount of uplift.

Over the center of the uplift, both hoop and radial stresses remain extensional throughout the rise of the diapir (Figure 7*b*). Hoop stresses are larger in magnitude, predicting formation of radial extensional features during uplift. As the diapir nears the surface, a zone of radial compressional stresses develops along the base of the growing region of uplift (Figure 7*b*, middle). Since hoop and radial stresses are opposite in sign and comparable in magnitude, strike-slip faulting is expected. As the diapir continues to near the surface (Figure 7*b*, bottom), compressional radial stresses at the base of the uplifted region have become large compared to hoop stresses, predicting formation of concentric compressional features.

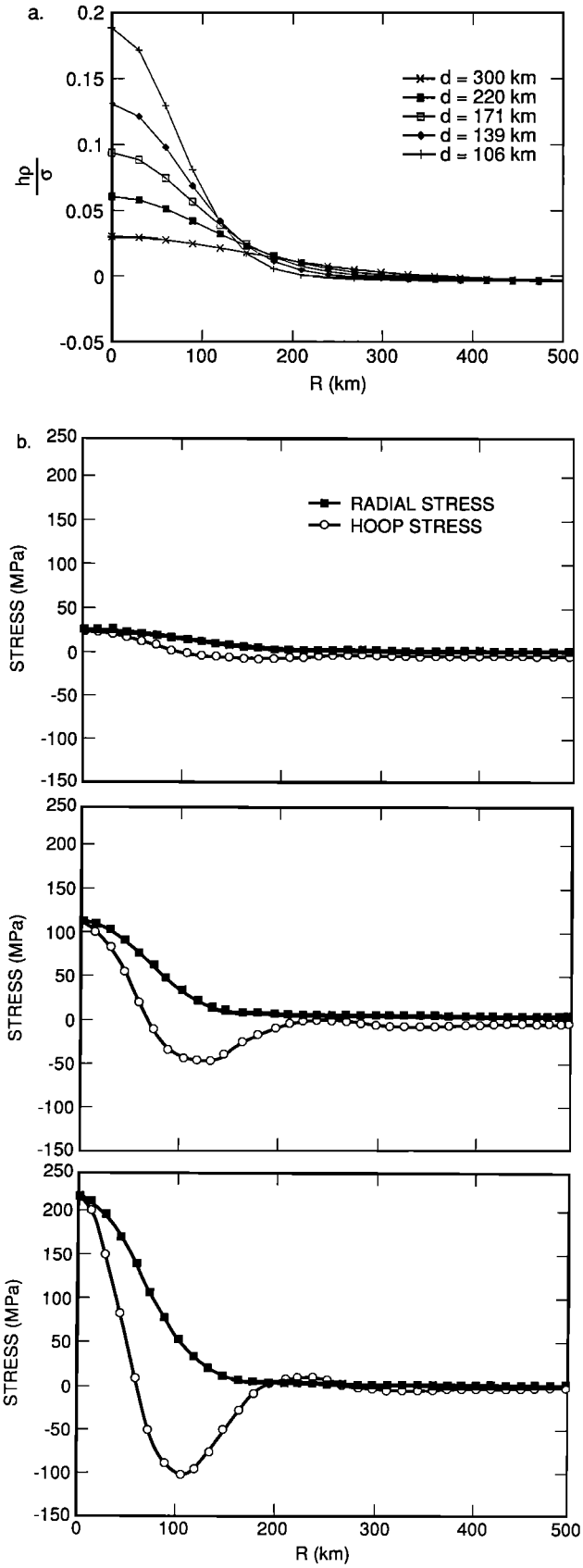

Fig. 7. Rising mantle diapir model results. (*a*) Surface topography shown at five different depths of the diapir. As the diapir approaches the surface, uplift increases and narrows. The topography results are scaled by the ratio of the density anomaly which represents the diapir (expressed as a surface mass density) to the density of the crust. For example, for a riser stress of about 30 MPa and a crustal density of 3000 kg m^{-3}, a dimensionless height of 1 is equal to 1 km. (*b*) Stress at the surface due to a rising mantle diapir. Radial, hoop, and vertical stresses are shown at three depths of the diapir; (top) depth = 220 km, (middle) depth = 171 km, and (bottom) depth = 106 km.

Variations of model parameters within the limits described above do not alter the prediction of radial extension in the interior of the uplifted region and strike-slip faulting along the periphery. Relative magnitudes of radial compression and azimuthal (hoop) extension along the periphery of the uplifted region depend on the strength (viscosity) structure of the lithosphere, which is a function of thermal gradient, crustal thickness and flow laws chosen for crust and mantle material. The magnitude of radial compression is increased for strong, thin near-surface layers, which is likely to occur for moderate to high (< 20 K km^{-1}) thermal gradients or increased (> 10 km) crustal thickness.

In summary, the hotspot or rising mantle diapir model predicts uplift of the surface, with the uplifted region becoming narrower and higher as the diapir approaches the surface. Radial normal faults are predicted over the center of the uplift with azimuthal compression or strike-slip faulting at the margins. Increasing the thermal gradient or the crustal thickness results in crustal thinning, decreased uplift, and increased azimuthal compression.

Sinking Mantle Diapir Model

The process by which a portion of the lower lithosphere detaches and sinks is extremely complex; thus its effects on the surface cannot be addressed in a simple model as was done for the rising mantle diapir. The process of a sinking mantle diapir can be broken into three stages (Figure 8):

Stage 1. An instability develops at the base of the thermal lithosphere due to cooling or at depth due to a phase change, leading to the detachment of material forming a sinking diapir (Figure 8*a*). Understanding the early time variations in surface topography and deformation as the instability develops and begins to detach involves a greater complexity of calculation than warranted here. Qualitatively, this stage is expected to lead to the formation of a topographic low and compressional tectonic features due to downward vertical normal stresses associated with the formation and initial detachment of the sinking body.

Stage 2. The detachment and sinking of a portion of the lithosphere produces three distinct sources of topography: upward vertical normal stresses associated with isostatic adjustment to hot material that has replaced the sinking body, downward vertical normal stresses associated with the sinking of the detached part of the lithosphere, and downward vertical normal stresses associated with loading of the surface by volcanism (Figure 8*b*). The shape of topography and the stress field depend on the interactions of these sources of stress and the rate at which each changes with time. Effects due to the sinking body are strongly attenuated as it sinks and thus depend upon its downward velocity. The rate at which the surface responds isostatically to hot material intruded at the base of the lithosphere or to a topographic load caused by volcanism depends primarily upon the viscosity of the mantle and the characteristic wavelength of the load. Also relevant is the characteristic thermal

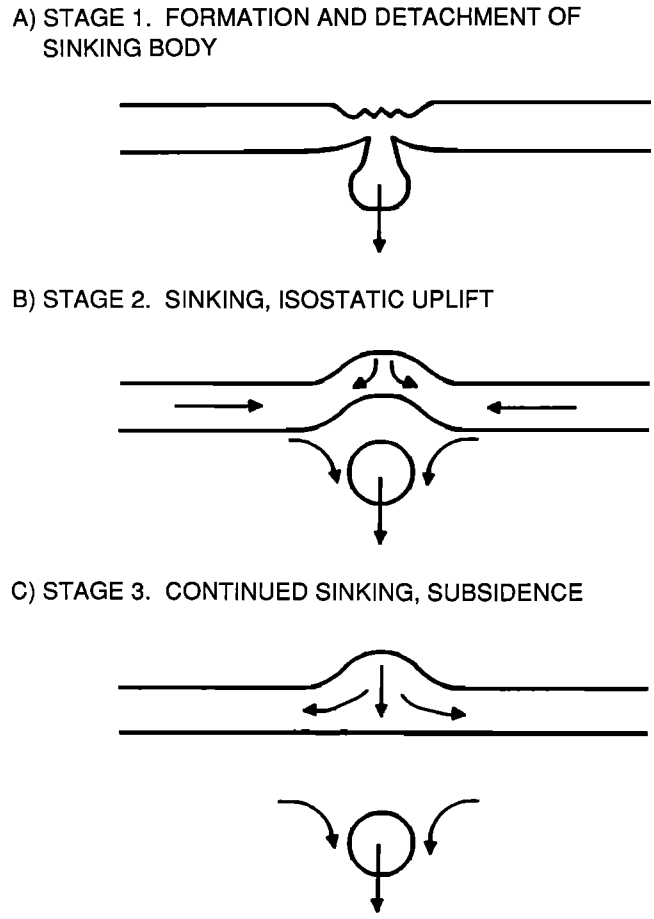

Fig. 8. Stages in the evolution of a sinking mantle diapir. (*a*) Stage 1. Formation and detachment of a portion of the lower lithosphere. A topographic low with interior compression is predicted. (*b*) Stage 2. Sinking of the body with isostatic uplift caused by replacement of the sinking portion of the lithosphere with warmer material. A trough is predicted around the uplift. This stage would most likely be accompanied by volcanism. (*c*) Stage 3. Continued sinking of the detached portion of the lithosphere, accompanied by subsidence of the topography and accompanying deformation. At this stage, crustal thickening would also occur.

relaxation time, which determines the rate at which thermal support for topography decreases. In order to assess the relative importance of these effects, we derive the characteristic time scales associated with each source of topography.

Consider a portion of the lithosphere that has detached and begun to sink due to its negative buoyancy. The mean temperature of the lithosphere is T_L and that of the convecting mantle below is $T_L + \Delta T$. The temperature difference ΔT leads to a density difference $\Delta\rho = \rho\alpha\Delta T$, where $\alpha = 3 \times 10^{-5}$ K^{-1} is the coefficient of thermal expansion and ρ is the density of mantle material at temperature T. To first order we ignore the details of the shape of the sinking body, and consider it as a sphere that obeys Stokes' law as it sinks. The diameter of the body divided by the sinking velocity yields a characteristic sinking time

$$\tau_D = \frac{9\mu_m}{\Delta\rho g a} \quad (1)$$

where μ is the viscosity of the convecting mantle, g is the acceleration due to gravity, and a is the characteristic radius of the sinker.

Uplift of the surface due to the intrusion of warmer mantle material into the void left by the sinking body occurs at a rate governed by the time constant for isostatic rebound, familiar from studies of glacial rebound [e.g., *Turcotte and Schubert,* 1982]. In the limit that load wavelengths are greater than lithospheric thickness (most coronae are greater than 250 km across):

$$\tau_r = \frac{\pi\mu}{\rho g a} \quad (2)$$

where $4a$ is taken to be the characteristic wavelength of the load. Since the load of any volcanic deposit associated with a corona is likely to be the same size (within a factor of a few), the same characteristic time scale applies to relaxation of such a load. Note that τ_D and τ_r are proportional to μ/a, and thus their ratio is constant even if mantle viscosity or sinking body radius are varied.

Cooling of the thermal intrusion beneath the surface (Figure 8) is governed by transient one-dimensional cooling and is characterized by a time scale

$$\tau_C = \frac{\Delta L}{\kappa} \quad (3)$$

where ΔL is the vertical dimension of the region where lithosphere has been replaced by warmer mantle material and κ is thermal conductivity. We first consider the case where $\Delta L = 2a$, adopting the parameters shown in Table 1. For these parameters, we find that $\tau_C > \tau_D$ as long as $a > 23$ km. The effect of our approximations is likely to overestimate τ_C and underestimate τ_D, but while a length scale of the order of 20 km could represent the thermal lithosphere on Venus (particularly postdating a delamination event, as supposed here), it is a factor of ~5 smaller than the smallest corona radius. More indicative is an example in which we take $L = 50$ km and $a = 100$ km. We then find $\tau_C = 83 \times 10^6$ years and $\tau_D = 17 \times 10^6$ years. For these same parameters, $\tau_r = 35{,}000$ years.

We therefore expect that the second stage of the sinking process will be accompanied by uplift of the surface and by deformation similar to that predicted by the rising diapir model. This uplift occurs rapidly compared to the sinking of the diapiric body and cooling of the intrusion of warm mantle material. The uplift is surrounded by a peripheral trough due to sinking of the detached portion of the lithosphere. As the diapir sinks and the heated mantle cools, it seems likely that the rise of warm mantle material to relatively shallow depths will result in partial melting, intrusion, and extrusion of melts. Because of the relatively long-lived nature of the thermal anomaly associated with delamination, volcanism and plutonism are expected to continue into the third stage of the sinking process.

Table 1. Model Parameters

Symbol	Parameter	Value
α	coefficient of thermal expansion	3×10^{-5} K^{-1}
a	radius of sinker	variable
ΔT	temperature difference between lithosphere and convecting mantle	200 K
ρ	density of lithospheric material at temperature T	3300 kg m^{-3}
κ	thermal conductivity	10^{-3} m s^{-2}
μ_m	viscosity of mantle at temperature $T + \Delta T$	10^{21} Pa s

Stage 3. At this point in the sinking process, a topographic high would exist on the surface due to thermal uplift, the sinking body would be near enough to the surface to have an effect on topography and stress fields, and volcanism would be likely to occur (Figure 8*c*). We therefore consider a model for this stage in which a sinking body and a volcanic load at the surface combine to produce topography and surface deformation. We use a version of the rising mantle diapir model modified to include an initial topographic load on the surface. Similar cases were run for the model: crustal thicknesses of 10 and 30 km; thermal gradients of 10, 20, and 30 K km^{-1}; and characteristic stresses of 10 and 25 MPa. We assumed that the sinking body was 200 K cooler than the mantle through which it sank, and for all models the initial topographic load due to volcanism was taken to be Gaussian in shape with an amplitude of 500 m. The initial depth of the sinking body was taken to be 100 km; runs were continued until a depth of 300 km was reached at which point the only significant change with increasing depth was an overall decrease in surface horizontal stress levels.

The combined vertical loads of the sinking body and the volcanic load result in the initial formation of a topographic trough surrounding the assumed topographic high (Figure 9). Figure 9 illustrates a nominal case which assumed a 30 km thick crust, 20 K km^{-1} surface thermal gradient, and 10 MPa characteristic stress. Relaxation of the topographic high occurs quite rapidly. This is consistent with the relationship between τ_r and τ_D as derived in equations (1) and (2). The bottom of the trough moves inward and the trough shallows as the diapir sinks and the topographic high relaxes. Although details of the topographic shape are different for different values of crustal thickness, thermal gradient, and characteristic stress, all cases exhibited a trough surrounding a high, which moved inward and shallowed while the topographic high relaxed. In all cases the maximum depth of the trough was approximately 100 m or less. This model implies that troughs are transient features; troughs around coronae also might be produced by flexure of the lithosphere.

The deformation due to the interaction of stresses due to a sinking body and a topographic load is complex, showing a great deal of variation both with time and with different values of model parameters. We summarize preliminary results here, with the caveat that more extensive examination would be required to fully characterize the processes that produce the deformation. The general pattern of stresses in the

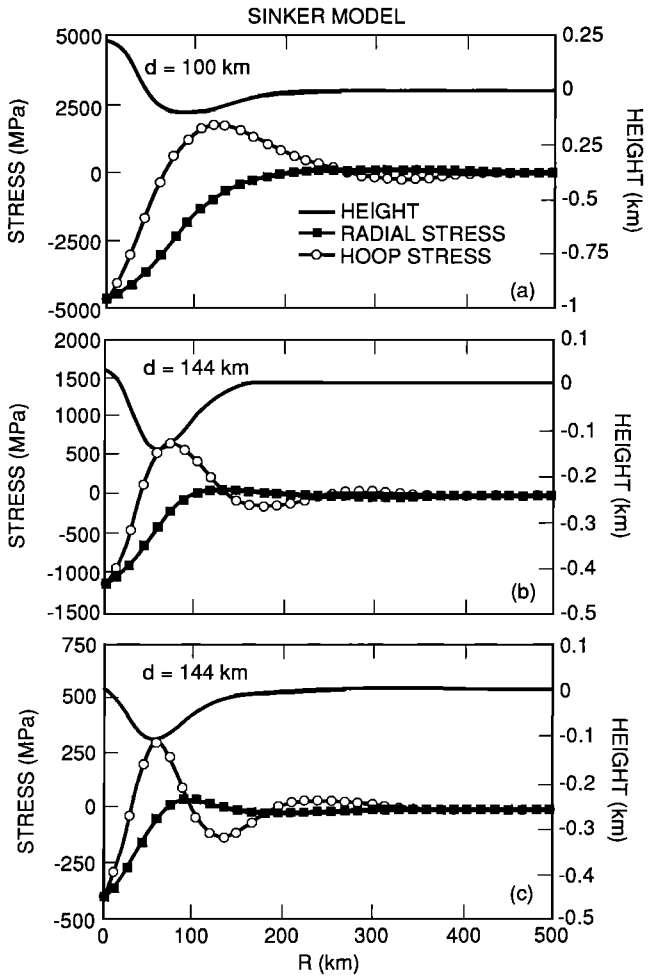

Fig. 9. Surface topography and stresses predicted by the sinking mantle diapir model for three depths of the sinking mantle diapir. As the diapir sinks, topography decreases and the trough shallows and narrows. The topography results are scaled by the ratio of the density anomaly which represents the diapir (expressed as a surface mass density) to the density of the crust. For example, for a sinker stress of about 30 MPa and a crustal density of 3000 kgm^{-3}, a dimensionless height of 1 is equal to 1 km. Shortening is predicted within the relaxing topographic high, with marginal radial extension that follows the trough as it moves inward as the diapir sinks. Radial compression occurs at later stages.

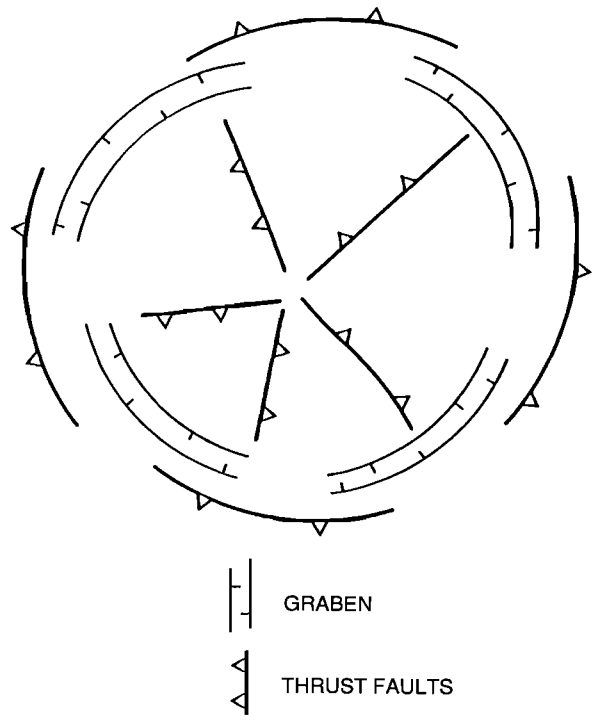

Fig. 10. Deformational features predicted by the sinking mantle diapir model. Interior radial compressional features are surrounded by concentric graben associated with the peripheral trough. Concentric compressional features are predicted to form outside the trough.

sinking mantle diapir model implies an inner zone of radial compressional features associated with the high topography of the volcanic load, a zone of concentric extensional features associated with the trough itself, and a zone of concentric compression surrounding the trough (Figures 9 and 10). The innermost zone is due the combined effects of the sinking body and the topographic load; both tend to cause compressional hoop and radial stresses at the center of the load. The zone of extension related to the trough is due to the surface load, which causes stress similar to that of an elastic layer. The outer zone of radial compression appears to be due to flow inward toward the center, related to the sinking body.

In summary, the sinking mantle diapir model is characterized by an early time depression with interior compression. This stage is followed by uplift of the surface surrounded by a trough, with radial extensional features and possibly peripheral compression. Uplift occurs rapidly compared to the sinking of the diapiric body and the cooling of intruded warm material. As the detached portion of the lithosphere continues to sink, the topographic high produced in the second stage relaxes. The trough around it shallows and narrows as sinking proceeds. Deformation produced by this final stage is characterized by radial compressional features associated with the interior high topography, concentric graben associated with the trough and compressional features surrounding the trough.

Gravitational Relaxation Model

Coronae represent a topographic load on the surface of Venus. The dominance of volcanic features indicates that some portion of corona topography consists of volcanic material deposited on the surface of the planet. In addition, thermal support for topography will decay as lithosphere heated by upwelling or delamination cools. Dynamic support will cease as a rising diapir encounters the rheological lid of the lithosphere. Gravitational relaxation of topography is a process that has been suggested as likely to occur on Venus on geologic time scales [*Weertman*, 1979; *Solomon et al.*, 1982*a*]. Materials at relatively shallow depths are expected to exhibit ductile flow due to high Venus surface temperatures. *Solomon et al.* [1982*a*] suggested that an impact basin several hundred kilometers across and 3 b.y. old or

greater should have little topographic relief at present. *Stephens et al.* [1983] predicted that the high topography of Maxwell Montes (over 8 km above the mean planetary radius (6051.9 km)) would relax in a few hundred million years if not supported by dynamic processes. At these time scales, and in the absence of significant erosion rates [*Ivanov et al.*, 1986], gravitational relaxation may be of great importance in modifying and reducing surface relief on Venus.

We apply a gravitational relaxation model to two topographic forms that might represent early forms of coronae on Venus, a dome and a plateau. The topographic forms are relaxed over time in an attempt to reproduce coronalike topography. In addition, stresses produced by the relaxing topography are analyzed to see if they are consistent with corona tectonic features.

The relaxation model uses the same layered rheology as the rising mantle diapir model [*Bindschadler and Parmentier*, 1990] (Figure 6). Solutions are those obtained by *Bindschadler* [1990], extended to axisymmetric geometries using two-dimensional FFTs. In all cases examined, shear stresses vanish at the surface. Relaxation is driven by topographic loads at the surface and/or crust-mantle boundary, which are approximated as discontinuities in vertical normal stress. Analytic solutions for topography and stresses are obtained as a function of time.

Two topographic forms were chosen as likely starting conditions for a corona: (1) a steep-sided topographic high or plateau and (2) a gently sloping topographic high or dome. Two starting conditions were used for each topographic form: (1) initially isostatically (Airy) compensated topography and (2) initially uncompensated topography

For the cases of an initially isostatically compensated plateau and dome, the topographic feature relaxes uniformly to zero (Figures 11*a* and 11*b*). Heights for the dome and plateau are equal to one at t=0. The topographic high does not undergo any significant change in form as it relaxes; the elevation decreases at approximately the same rate for all wavelengths. The model fails to reproduce the trough characteristic of most coronae, as well as the central low typical of many coronae.

Relaxation of initially isostatically uncompensated topography results in the more rapid lowering of the feature and development of a peripheral trough (Figure 12). Relaxation of a plateau results in the formation of a central low, while relaxation of a dome does not. The topography of the relaxed structure is similar to

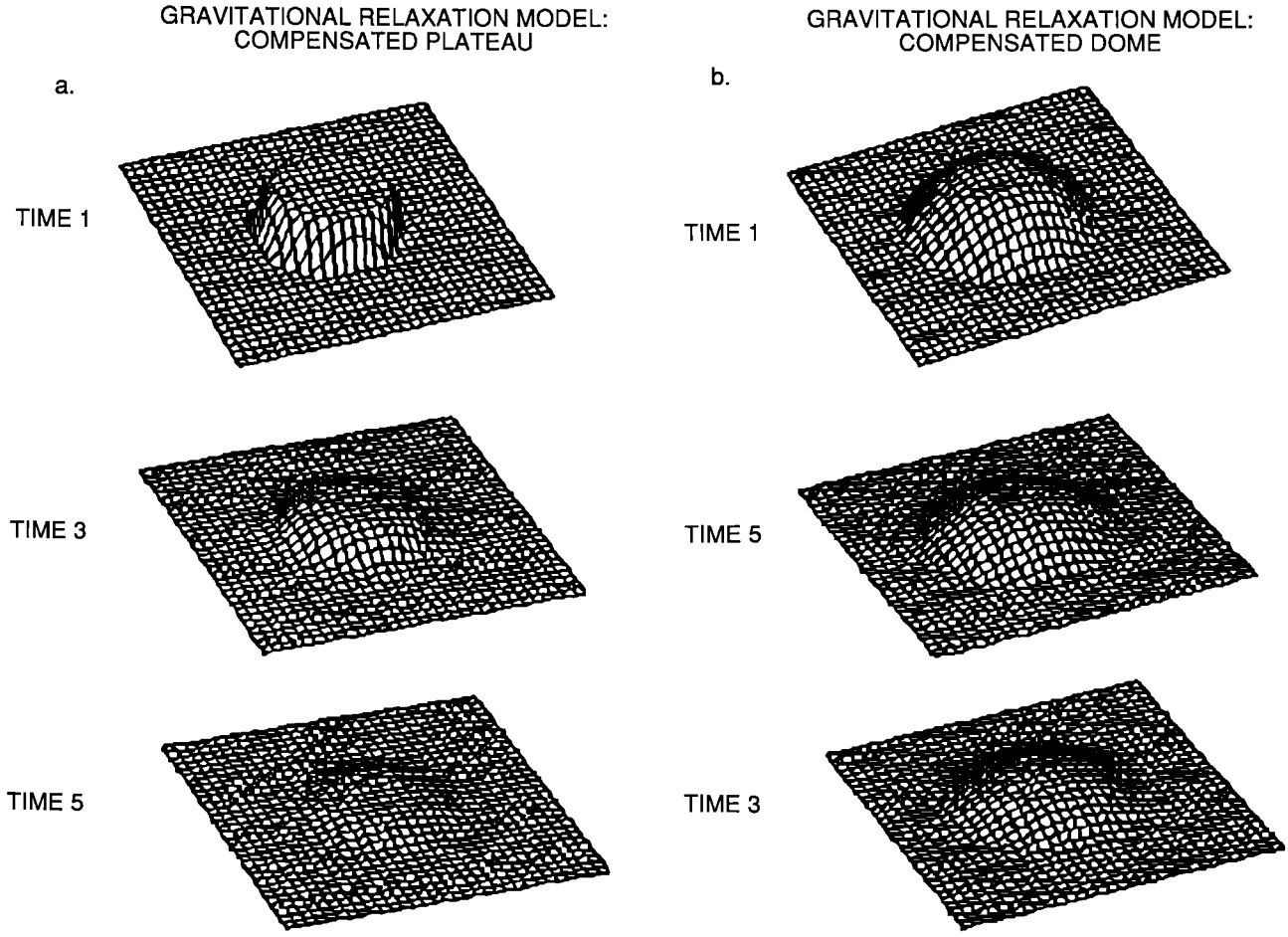

Fig. 11. Topography resulting from gravitational relaxation of an initially isostatically compensated (*a*) plateau and (*b*) dome. The initial form of the topography is preserved as the topographic relief decreases, shown for three arbitrary time steps.

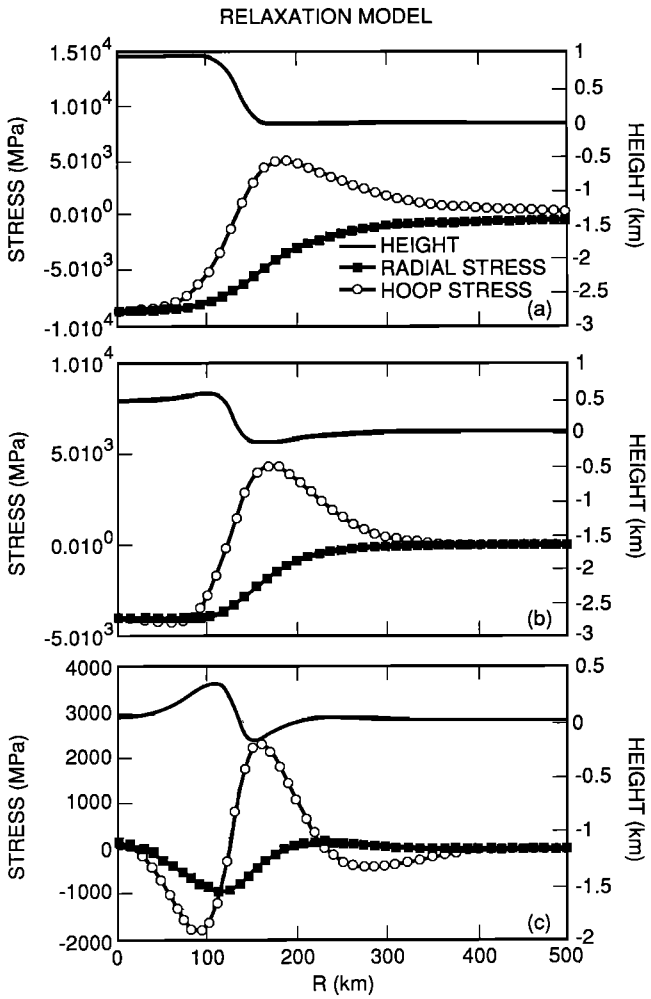

Fig.12. Topography and stresses predicted by the relaxation of an uncompensated plateau. Results for the dome are similar. Topography, vertical, hoop and radial stress are shown, at (*a*) 260 years, (*b*) 5700 years, and (*c*) 25,000 years. As the topographic high lowers in relief, a central sag and peripheral trough develop. Relaxation occurs on more rapid time scales than in the compensated case. Uncompensated relaxation of a dome resembles Figure 11*b*; no central sag is formed, although a trough does form. Stress levels are quite high due to the high viscosity of near-surface layers. As time proceeds, the shape of the stress curves remains approximately the same, until very late stages when the stress levels are extremely low and the relaxation more resembles that of compensated topography.

that of a relaxing impact crater [*Solomon et al.*, 1982*a*, *b*; *Hall et al.*, 1981]. Relaxation proceeds at an initially faster rate than the compensated cases, as much of the deformation is taken up in the relatively inviscid half-space. Early time stresses for the uncompensated cases are much higher than in the compensated cases. Plots of surface stress for the plateau (Figure 12) indicate that at early times, the center of the plateau undergoes both radial and azimuthal compression, while radial extension occurs along the base of the plateau. As relaxation progresses, compressional stresses in the center decrease, hoop stresses decrease in magnitude, radial compressional stresses are focused along the rim, and radial extensional stresses are focused in the developing trough. If the thermal gradient is decreased (and the thickness of the rheological lithosphere increased), initial compression in the center of the feature becomes greater compared to later extension, as more of the earlier deformation is taken up in sagging of the strong layer [*Bindschadler*, 1990].

The topographic form and stresses resulting from gravitational relaxation differ based on the initial degree of isostatic compensation of the topographic feature. Initially uncompensated domes and plateaus undergo a change in shape as they relax, forming peripheral troughs, and, in the case of the plateau, central sags. Stresses are initially compressional in the center and extensional at the periphery, then change in sign and decrease in magnitude as relaxation proceeds. Initially compensated features maintain their shape as they relax.

Discussion

Model Predictions

We have formulated and tested three models that may be involved in corona origin and evolution: mantle diapirism (rising and sinking anomalies) and gravitational relaxation of topography.

Hotspot model. A hotspot or rising mantle diapir produces uplift at the surface, with extensional radial features predicted in the central region surrounded by azimuthal compressional features. Higher, narrower uplift is produced as the rising diapir is placed nearer to the surface.

Sinking diapir model. For a sinking mantle diapir, an initial depression is predicted followed by uplift and volcanic loading. A peripheral trough is predicted, along with an inner zone of radial thrusting, concentric graben associated with the trough, and concentric features of compressional origin surrounding the trough.

Gravitational relaxation. The gravitational relaxation model was tested for several cases of initial isostatic compensation for a plateau and dome. In the initially compensated case, both the plateau and dome relax without a change in shape. The initially uncompensated case does predict a change in shape, with a peripheral trough and central sag produced as the dome or plateau relaxes. The central region is initially characterized by both radial and azimuthal compression. As the plateau changes shape, radial compression is focused along the rim and radial extension in the trough surrounding the plateau.

Comparisons to Corona Characteristics

In the hotspot model, early uplift and central extension are predicted, consistent with the swell-like topography, tectonic features, and central volcanism characteristic of coronae. The peripheral trough and central low region typical of many coronae are consistent with uncompensated relaxation of the uplifted region. The central low characteristic of many coronae is only produced by the uncompensated relaxation model. The hotspot or rising mantle diapir model does predict that the topography narrows as the anomaly approaches the surface. Late stage behavior of the rising mantle diapir, when flattening occurs as

the body approaches the surface, may cause additional deformation not included in this model. No correlation between age or complexity of structure and size of coronae has been identified at this time. In general, the hotspot model combined with gravitational relaxation is consistent with most of the major characteristics of coronae. This combination of models predicts relatively late stage formation of the central low and trough.

A sinking mantle diapir model would produce an initial depression followed by uplift and trough formation. The predicted topography is consistent with coronae, with the exception of the lack of identification of basins that may be precursors to coronae. As the diapir sinks, the peripheral trough narrows and shallows. Troughs surrounding coronae are generally 50-75 km across and approximately 500 m deep, with no obvious change with increasing corona degradation. Coronae interpreted to be the oldest (those in the subdued class) are not surrounded by troughs, which could, however, be below the resolution of available altimetry data [*Pronin and Stofan,* 1990]. Or the troughs around these coronae may be infilled with volcanic material. Radial compressional features, concentric graben, and outer concentric compression are predicted at corona. Concentric graben are not typical of coronae in the Venera 15/16 data, and the concentric compressional features lie outside the trough unlike at coronae. Some interior linear features are of unknown origin and thus may fit the model. The raised topography produced in this model would undergo gravitational relaxation as described above. In general, the sinking mantle diapir can account for many of the observed corona characteristics, but the prediction of dominant central thrusting, concentric graben, outer concentric compressional features, and an early time topographic low makes it a less favored model. Neither model adequately explains why deformation is concentrated in the annulae of coronae.

The average age of the surface of the northern hemisphere of Venus has been estimated at 0.5-1.0 b.y. [*Ivanov et al.,* 1986] or younger [*Schaber et al.,* 1987]. Since gravitational relaxation is a time-dependent process, upper limits can be placed on the age of coronae. For a mantle viscosity of 10^{21} Pa s, relaxation time for a 400-km-diameter uncompensated plateau is approximately 100 m.y. or less [*Bindschadler,* 1990]. Relaxation times for compensated features will be longer, and are sensitive to crustal thickness and temperature gradient. These relatively fast relaxation time scales suggest that many coronae are relatively young in age, with most probably similar in age to the overall age of the northern hemisphere. The process of corona formation appears to have been occurring over a period of time, with some coronae apparently almost completely relaxed (e.g., Demeter), others in the process of relaxation (e.g., Feronia), and others still may be forming (e.g., protocoronae).

Conclusions

We have developed models that can be used to predict topography and stresses resulting from forces caused by a mantle diapir at depth acting on layers of prescribed viscosity. In the hotspot or rising diapir model, uplift is accompanied by central extensional features surrounded by azimuthal compressional features. As the force distribution representing the diapir is placed closer to the surface, narrower higher uplift results along with radial normal faulting and some amount of concentric compression. The sinking mantle diapir model predicts uplift of the surface surrounded by a peripheral trough. The high topography increases and the trough narrows and shallows as the diapir is placed at deeper levels. Radial thrust faults, concentric graben, and outer concentric compressional features are predicted. Gravitational relaxation models were also investigated and were found to produce a central topographic low and peripheral trough.

Origin of Coronae

Coronae on Venus have several defining characteristics including relatively raised topography, annuli of concentric ridges, peripheral troughs, and association with volcanism. Studies of individual corona morphology have defined a sequence of events. Uplift and volcanism occur in the early stages, followed by annulus and trough formation, topographic degradation, and continued volcanism. This sequence of events is most consistent with formation by a hotspot accompanied and followed by gravitational relaxation. However, the sinking mantle diapir model cannot be completely ruled out, as it predicts many features characteristic of coronae. None of the models adequately explains formation of the annulus. We are currently developing more detailed relaxation models as well as examining other possible mechanisms of annulus formation.

Relaxation time scales suggest that some coronae are relatively young features. The process of corona formation is an ongoing one; some structures appear highly degraded, and others still may be in the process of formation. Variations in morphology between coronae are interpreted to result from differences in their individual stage of evolution as well as differences in the significance of various processes in their evolution. Coronae occur as both isolated features in the low- latitude plains and in clusters at higher latitudes. Regardless of whether coronae formed by rising or sinking mantle diapirs, their formation involved a significant transfer of heat from the interior to the surface. We are currently assessing the significance of coronae to heat loss processes, as well as their relationship to global tectonic patterns.

Tests for Magellan

High resolution image and altimetry data from the Magellan mission to Venus which arrived in mid-1990, can be used to differentiate between models of corona origin. The sequence of events, initial topography and evolution of the trough, and nature of interior tectonic features are critical in understanding corona formation.

Sequence of events. The rising mantle diapir model predicts early uplift and volcanism followed by later trough formation. The sinking model predicts

formation of a topographic low, followed by a topographic high surrounded by a trough. Formation of a compressional annulus could occur at early stages or at later stages outside the trough. At present, the geological relations that have been established [*Stofan and Head,* 1990; *Pronin and Stofan,* 1990] are not sufficiently detailed to permit distinguishing between the two models. Volcanic complexes interpreted as proto-coronae and coronae such as Bachue suggest that uplift and volcanism predate major annulus and trough formation, favoring the hotspot model.

Topography. Detection of basins which may be precursors to coronae in the Magellan data would provide support for the sinking diapir model. In addition, the sinking mantle diapir model predicts that the trough will become more narrow and shallow with time. Neither of these effects has been identified in available (50-100 km resolution) altimetry data. Current data suggest that the troughs around coronae are all about the same width and depth, which supports the predictions of the gravitational relaxation model.

Interior tectonic features. Many ridges in the interior of coronae are of unknown origin. An extensional origin for the features would support the hotspot model, while a compressional origin would support the sinking diapir model. In addition, the hotspot model predicts that the topography will narrow and become higher as the anomaly approaches the surface. No correlation between complexity of structure and size has been determined, but higher resolution images of the deformed interior of many coronae may permit detection of this effect. The study of the interior of coronae and their evolution and topographic characteristics with high-resolution images and altimetry from Magellan should allow us to distinguish between models of origin. In addition, more complex models analyzing effects of flattening of the diapir as it approached the surface are needed.

Gravity signature. Hotspots on the Earth have a characteristic gravity signature (positive geoid anomalies). Magellan gravity data will be used to determine if coronae have a characteristic gravity signature and how it compares to the gravity signatures of terrestrial hotspots.

Acknowledgments. This work was supported by NASA grants NAGW-713, NGR40002088, and JPL contract 957088, as well as the William F. Marlar Foundation. One of the authors (E.R.S.) was supported by a NASA Goddard Space Flight Center Graduate Student Fellowship. We gratefully acknowledge helpful discussions with Alex Pronin, A.T. Basilevsky, Ray Fletcher, Carle Pieters, and Pete Schultz. We would like to thank helpful reviews by Bob Grimm and an anonymous reviewer.

REFERENCES

Anderson, E.M., The dynamics of faulting and dyke formation, with applications to Britain, 2d ed., Oxford Press, Edinburgh, 1951.

Barsukov, V.L., *et al.*, The geology and geomorphology of the Venus surface as revealed by the radar images obtained by Veneras 15 and 16, *J. Geophys. Res.*, *91*, 378-398, 1986.

Basilevsky, A.T., A.A. Pronin, L.B. Ronca, V.P. Kryuchkov, A.L. Sukhanov, and M.S. Markov, Styles of tectonic deformation on Venus: Analysis of Veneras 15 and 16 data, *J. Geophys. Res.*, *91*, 399-411, 1986.

Bindschadler, D.L., Models for the origin of tessera terrain: A study of the tectonics of Venus, Ph.D. thesis, 241 pp., Brown University, Providence, R.I.,May, 1990.

Bindschadler, D.L., and E.M. Parmentier, Mantle flow tectonics and a ductile lower crust: Implications for the formation of large-scale features on Venus, *J. Geophys. Res.*, *95*, 21,329-21,344, 1990.

Campbell, D.B., J.W. Head, J.K. Harmon, and A.A. Hine, Venus: Identification of banded terrain in the mountains of Ishtar Terra, *Science*, *221*, 644-647, 1983.

Crumpler, L.C., J.W. Head, and D.B. Campbell, Orogenic belts on Venus, *Geology*, *14*, 1031-1034, 1986.

Frank, S. L., and J.W. Head, Classification of Class II ridge belts on Venus (abstract), *Lunar Planet. Sci., XIX*, 351-352, 1988.

Goetze, C., The mechanisms of creep in olivine, *Philos. Trans. R. Soc. London, Ser. A, 288*, 99-119, 1978.

Grimm, R.E., and S.C. Solomon, Viscous relaxation of crater relief on Venus: Constraints on crustal thickness and thermal gradient, *J. Geophys. Res.*, *93*, 11,911-11,929, 1988.

Hall, J.L., S.C. Solomon, and J.W. Head, Lunar floor-fractured craters: Evidence for viscous relaxation of crater topography, *J. Geophys. Res.*, *86*, 9537-9552, 1981.

Head, J.W., and L. Wilson, Volcanic processes and landforms on Venus: Theory, predictions and observations, *J. Geophys. Res.*, *91*, 9407-9446, 1986.

Ivanov, B.A., A.T. Basilevsky, V.P. Kryuchkov, and I.M. Chemaya, Impact craters of Venus: Analysis of Veneras 15 and 16 data, *J. Geophys. Res.*, *91*, 413-430, 1986.

Kryuchkov, V.P., The feature length and spacing comparison among ridge and groove belts, coronae, and mountain surrounding of Lakshmi, II (abstract), *Lunar Planet. Sci., XIX*, 651-652, 1988*a*.

Kryuchkov, V.P., Ridge belts on the plains of Venus, I (abstract), *Lunar Planet. Sci., XIX*, 649-650, 1988*b*.

Masursky, H., Geological evolution of coronae (complex circular features) on Venus (abstract), *Lunar Planet. Sci., XVIII*, 598-599, 1987.

Pettengill, G.H., E. Eliason, P.G. Ford, G.B. Loriot, H. Masursky, and G.E. McGill, Pioneer Venus radar results: Altimetry and surface properties, *J. Geophys. Res.*, *85*, 8261-8270, 1980.

Pronin, A.A., and E.R. Stofan, Coronae on Venus: Morphology and distribution, *Icarus*, *87*, 452-474, 1990.

Schaber, G.G., E.M. Shoemaker, and R.C. Kozak, Is the Venusian surface really old? (abstract), *Lunar Planet. Sci., XVIII*, 874-875, 1987.

Shelton, G., and J. Tullis, Experimental flow laws for crustal rocks (abstract), *Eos Trans. AGU*, *62*, 396, 1981.

Solomon, S.C., and J.W. Head, Venus banded terrain: Tectonic models for band formation and their relationship to lithospheric thermal structure, *J. Geophys. Res.*, *89*, 6885-6897, 1984.

Solomon, S.C., S.K. Stephens, and J.W. Head, On Venus impact basins: Viscous relaxation of topographic relief, *J. Geophys. Res.*, *87*, 7763-7771, 1982*a*.

Solomon, S.C., R.P. Comer, and J.W. Head, The evolution of impact basins: Viscous relaxation of topographic relief, *J. Geophys. Res.*, *87*, 3974-3992, 1982*b*.

Stephens, S.K., S.C. Solomon, and J.W. Head, On the age of Venus highland topography: Constraints on the viscous relaxation of relief (abstract), *Lunar Planet. Sci., XIV*, 747-748, 1983.

Stofan, E.R., and J.W. Head, Pioneer Venus characteristics of ovoids on Venus: Preliminary results (abstract), *Lunar Planet. Sci., XVII*, suppl.,1033-1034, 1986.

Stofan, E.R., and J.W. Head, Coronae of Mnemosyne Regio, Venus: Morphology and origin, *Icarus.*, 83, 216-243, 1990.

Stofan, E.R., J.W. Head, and E.M. Parmentier, Corona structures on Venus: Models of origin (abstract), *Lunar Planet. Sci., XVIII*, 954-955, 1987.

Stofan, E.R., J.W. Head, and E.M. Parmentier, Corona

structures on Venus: Evidence for a diapiric origin (abstract), *Lunar Planet. Sci., XIX*, 1129-1130, 1988.

Turcotte, D. L., and G. Schubert, *Geodynamics: Application of continuum physics to geological problems*, 450 pp., John Wiley, New York, 1982.

Weertman, J., Height of mountains on Venus and the creep properties of rock, *Phys. Earth Planet. Inter.*, *19*, 197-207, 1979.

D.L. Bindschadler, Department of Earth and Space Sciences, UCLA, Los Angeles, CA 90024.

J.W. Head and E.M. Parmentier, Department of Geological Sciences, Box 1846, Brown University, Providence, RI 02912.

E.R. Stofan, Jet Propulsion Laboratory, MS 230-225, 4800 Oak Grove Drive, Pasadena, CA 91109.

(Received January 17, 1990;
revised August 27, 1991;
accepted August 27, 1991)